Two-dimensional spatial coherence of excitons in semicrystalline polymeric semiconductors: Effect of molecular weight

Francis Paquin,[1] Hajime Yamagata,[2] Nicholas J. Hestand,[2] Maciej Sakowicz,[1] Nicolas Bérubé,[1] Michel Côté,[1] Luke X. Reynolds,[3] Saif A. Haque,[3] Natalie Stingelin,[4] Frank C. Spano,[2,*] and Carlos Silva[1,†]

[1]*Département de physique & Regroupement québécois sur les matériaux de pointe, Université de Montréal, C. P. 6128, Succursale centre-ville, Montréal (Québec) H3C 3J7, Canada*

[2]*Department of Chemistry, Temple University, Philadelphia, Pennsylvania 19122, USA*

[3]*Department of Chemistry and Centre for Plastic Electronics, Imperial College London, South Kensington Campus, London SW7 2AZ, United Kingdom*

[4]*Department of Materials and Centre for Plastic Electronics, Imperial College London, South Kensington Campus, London SW7 2AZ, United Kingdom*

(Received 6 June 2013; revised manuscript received 19 September 2013; published 7 October 2013)

The electronic properties of macromolecular semiconductor thin films depend profoundly on their solid-state microstructure, which in turn is governed, among other things, by the processing conditions selected and the polymer's chemical nature and molecular weight. Specifically, low-molecular-weight materials form crystalline domains of cofacially π-stacked molecules, while the usually entangled nature of higher-molecular-weight polymers leads to microstructures comprised of molecularly ordered crystallites interconnected by amorphous regions. Here, we examine the interplay between extended exciton states delocalized along the polymer backbones and across polymer chains within the π stack, depending on the structural development with molecular weight. Such two-dimensional excitations can be considered as Frenkel excitons in the limit of weak intersite coupling. We combine optical spectroscopies, thermal probes, and theoretical modeling, focusing on neat poly(3-hexylthiophene) (P3HT)—one of the most extensively studied polymeric semiconductors—of weight-average molecular weight (M_w) of 3–450 kg/mol. In thin-film structures of high-molecular-weight materials ($M_w > 50$ kg/mol), a balance of intramolecular and intermolecular excitonic coupling results in high exciton coherence lengths along chains ($\sim$4.5 thiophene units), with interchain coherence limited to $\sim$2 chains. In contrast, for structures of low-M_w P3HT (<50 kg/mol), the interchain exciton coherence is dominant ($\sim$30% higher than in architectures formed by high-molecular-weight materials). In addition, the spatial coherence within the chain is significantly reduced (by nearly 25%). These observations give valuable structural information; they suggest that the macromolecules in aggregated regions of high-molecular-weight P3HT adopt a more planar conformation compared to low-molecular-weight materials. This results in the observed increase in intrachain exciton coherence. In contrast, shorter chains seem to lead to torsionally more disordered architectures. A rigorous, fundamental description of primary photoexcitations in π-conjugated polymers is hence developed: two-dimensional excitons are defined by the chain-length dependent molecular arrangement and interconnectivity of the conjugated macromolecules, leading to interplay between intramolecular and intermolecular spatial coherence.

DOI: 10.1103/PhysRevB.88.155202 PACS number(s): 71.35.Cc, 78.55.Kz, 78.66.Qn

I. INTRODUCTION

"Plastic" semiconductors are often regarded as complex systems as the conjugated macromolecules they are made of can adopt different arrangements and packing, leading to a diverse range of microstructures. These define their electronic properties. For instance, the chain conformation of conjugated polymers and the resulting microstructure has been shown to have a profound impact on the nature of intra- and interchain dispersion of π electrons.[1–10] Therefore it is essential to learn how to manipulate these structural features. One option is to select materials of different molecular weight. From a perspective of classical polymer science, it is well established that polymers of low weight-average molecular weight (M_w) form unconnected, extended-chain crystals, usually of a parrafinic-like arrangement. Due to the non-entangled nature of these relatively short-chain macromolecules, this leads to a polycrystalline, one-phase morphology. In contrast, with high-M_w materials of molecular weight larger than the molecular weight between entanglements (M_e), typically two-phase morphologies are obtained, which are comprised of crystalline moieties embedded in largely unordered (amorphous) regions, whereby individual macromolecules bridge multiple domains of order.[11]

Perhaps the central objective and challenge in the broad field of plastic electronics is to relate the electronic properties to the molecular order and thin-film architectures of the constituting materials; hence significant research efforts have been devoted to that endeavor. Regioregular poly(3-hexylthiophene) (P3HT) has emerged as a model material to investigate the relationship between macromolecular configuration, microstructure, and electronic properties. For example, charge transport in P3HT has been found to display clear trends with molecular weight and whether the film displays one-phase (polycrystalline) or two-phase (entangled) morphologies. In field-effect transistors, Kline *et al.* observed a systematic increase in field-effect mobilities up to a weight-average molecular weight of 40 kg/mol,[12–14] in agreement with reports by Zhang *et al.*[15] and Koch *et al.*[16] On the other hand, bulk mobilities display more complex trends with molecular

weight, and depend sensitively on film processing routes. Ballantyne *et al.* found, for instance, an order-of-magnitude decrease in bulk charge mobilities for P3HT of molecular weight $M_w > 18$ kg/mol.[17] Koch *et al.* reported maximum bulk mobilities for P3HT of $M_w \sim 4$ kg/mol. For materials of higher molecular weight, the time-of-flight mobility was found to be again reduced, leveling at a value of $\sim 10^{-4}$ cm^2/Vs.[16] However, when films were cast at 115 °C, the mobility *increased* by over an order of magnitude for materials of $M_w < 10$ kg/mol, and *decreased* by over two orders of magnitude for P3HT of $M_w \approx 60$ kg/mol.[16]

In this contribution, we focus on the nature of excitons in regioregular P3HT with molecular weights ranging from 3–450 kg/mol, where the microstructure changes from chain-extended crystals to a semicrystalline morphology in which amorphous and crystalline domains are interconnected.[3] This structural transition occurs at a molecular weight of around 25 to 35 kg/mol.[10,18] Our strategy is to exploit the intricate influence of electronic structure and spatially correlated energetic disorder on the spectral line shapes in order to extract the microstructure-dependent information on exciton coherence.[19–24] More specifically, our objective is to explore how the exciton coherence lengths, measured along the polymer backbone and across the π stack, vary with molecular weight and, in particular, with the structural change occurring above the entanglement limit. (The third dimension, which is directed along the lamellar axis, is neglected, as excitonic interactions are negligible between the well-separated π stacks.) Although exciton coherence lengths have been defined in various ways,[20–24] we adapt the definition from Ref. 23 and generalize it to two dimensions. In short, we seek the two-dimensional exciton coherence function as a function of polymer structure.

Conjugated polymers are structurally complex and can, among other things, feature torsional disorder along the backbone, which translates into site energy disorder. Furthermore, the π-electron coupling leading to electronic dispersion is highly anisotropic; dispersion along the chain is present due to intramolecular coupling between adjacent monomer motifs, but interchain coupling also clearly plays a role, leading to two-dimensional dispersion.[25,26] As a consequence, neutral excitations (containing an electron and hole) in this class of materials can be considered to be in the Frenkel limit with respect to interchain interactions, highly localized to a few lattice sites across the lamellar lattice, spanning $\sim$1 nm, and highly influenced by energetic disorder.[23]

Spano has previously described excitons in regioregular P3HT by invoking a weakly coupled H-aggregate model in which weak excitonic coupling (compared to molecular reorganization energies) between neighboring polymer chains within the π stack leads to electronic dispersion of the vibronic molecular levels to form vibronic bands, with the bandwidth strongly dependent on microstructure.[27,28] However, the importance of intrachain coupling on optical spectral signatures has become evident by a recent report of J-aggregate-like behavior in P3HT nanofibres[1] and in a P3HT:PEO complex[29] in which head-to-tail interactions of transition dipole moments of chromophores along the chain influence spectral line shapes. The limiting case of through-bond, intrachain excitonic coupling leads to what can be considered as Wannier-Mott-type excitons in one-dimensional lattices.[30,31] In such excitons, the electron and hole are bound over several unit cells. A compelling example of this limit is provided by isolated, extended chains of red-phase polydiacetylene derivatives,[31] which show ultranarrow photoluminescence linewidths and superradiance[32–34] characteristic of J aggregates at low temperature.[35] The work by Niles *et al.*[1] demonstrates that in regioregular P3HT films, there is a competition between J-like (intrachain) and H-like (interchain) excitonic coupling.[36] This interplay between through-bond and through-space excitonic coupling of adjacent chromophores must be strongly influenced by energetic disorder and hence the macromolecular conformation and packing in the solid state.

In what follows, we combine steady-state and time-resolved optical spectroscopy, thermal analysis and theoretical modeling based on an effective Frenkel exciton Hamiltonian introduced in Ref. 36 in order to unravel the interplay between through-bond excitonic coupling within polymer chains, and Coulombic coupling between adjacent chains within a π stack. Thus far, the result of such intrachain/interchain exciton coupling has been analyzed theoretically for the case of ordered aggregates with a thermal Boltzmann distribution of emitting excitons.[36] In this work, we find that the influence of intrachain versus interchain coupling on the photophysical response is strongly dependent on the microstructure imposed by processing and materials parameters such as molecular weight. In order to interpret such effects theoretically, we extend the analysis of Ref. 36 to the case of disordered aggregates. In the low-molecular-weight regime, the paraffinic-like chain-extended structures seem to lead to short chromophores that produce more strongly coupled H aggregates, very likely due to torsional disorder along the polymer backbone introduced, for example, through end-group effects.[11] On the other hand, films prepared with P3HT of molecular weight above the entanglement limit feature weaker interchain coupling but stronger intrachain coupling. We attribute this to the presence of longer-chain chromophore segments originating from torsionally more ordered (i.e., more planar) macromolecules. We thus find that the intrachain and interchain spatial coherence of excitons evolve with opposite trends with molecular weight, with longer intrachain coherence being observed for materials of high M_w, but longer interchain coherence in low-molecular-weight matter. The photophysical properties arise from the competition between intrachain (through-bond) electronic coupling characteristic of Wannier-Mott excitons and interchain (through-space) electronic coupling leading to Frenkel excitons, which generally dominate the photophysical properties of plastic semiconductors.

II. EXPERIMENTAL METHODS

P3HT films of weight-average molecular weight (M_w) in the range of 3–450 kg/mol were wire-bar-coated from p-xylene solution (1 wt% solid content) onto glass substrates. The solution temperature was 70 °C, and the substrate was also kept at 70 °C. Absorption spectra were measured using a commercial UV-Vis spectrophotometer (Perkin Elmer, Lambda25). The photoluminescence experiments were carried out by excitation with a continuous-wave laser (Ultralasers Inc., 200 mW

maximum, 532 nm) modulated at a frequency of 100 Hz with a mechanical chopper (Terahertz Technologies), detection with a 300-mm spectrometer (Princeton Instruments SP2300 with EOS model S/PBS-025/020-TE2-H photoreceiver), and phase-sensitive detection (SR830 lock-in amplifier). The sample was housed in a closed-cycle, temperature controlled, sample-in-vapor cryostat (CryoIndustries of America).

The ultrafast time-resolved PL measurements were performed by femtosecond fluorescence upconversion. The samples were excited by the frequency-doubled output from an ultrafast mode-locked Ti:Sapphire oscillator (Newport Spectra-Physics Broadband MaiTai). Excitation and gate wavelengths were fixed at 400 and 800 nm, respectively. Both the gate and excitation beams were independently compressed using prism-pair compressors. The excitation intensity was adjusted to be below the onset of intensity-dependent kinetics. Photoluminescence from the sample was focused on a 200-μm-thick BBO crystal along with the 800-nm gate beam. Sum frequency generated photons (corresponding to photoluminescence at either 650 or 720 nm) were detected using a photomultiplier tube (R7207-01, Hamamatsu). The temporal resolution of the system was less than 150 fs. Sample degradation was avoided by performing the measurements under flowing nitrogen and using a translation stage to constantly move the sample within the beam, removing the effect of photobleaching and providing data averaged across the whole of the sample.

Melting temperatures T_m and enthalpies of fusion ΔH_f were determined with a Mettler DSC822e differential scanning calorimeter (DSC), calibrated with indium and zinc. Samples of 1–5 mg (obtained from thin-film structures cast from solution following an identical protocol as for optical measurements) were sealed in aluminum crucibles and then heated under nitrogen at a scanning rate of 10 °C/min. Enthalpies of fusion were deduced from the surface area underneath the melting endotherms.

III. RESULTS AND ANALYSIS

A. Relationship between exciton signatures and solid-state microstructure

In this section, we explore the dependence of steady-state absorption and photoluminescence (PL) spectral line shapes of P3HT films with M_w. Figure 1(a) displays the room-temperature absorption spectra of films of P3HT of two different M_w; one prepared with P3HT of low-M_w (12.4 kg/mol) and one made of high-M_w material (264 kg/mol). We discern two distinct differences in the spectral line shapes of these samples. The first concerns the relative absorbance of the origin of the vibronic progression at 2.0 eV. As mentioned in Sec. I, previous work by Spano has demonstrated that the absorption line shape can be understood within the framework of a weakly coupled H-aggregate model.[5,6,27] Weak resonant Coulombic coupling between cofacial polymer chains, J_{inter}, results in electronic dispersion of the vibronic molecular levels to form vibronic bands with free-exciton bandwidth $W = 4J_{inter}$. W is related to absorbance ratio of 0-0 and 0-1 peaks at 2.0 and 2.2 eV, respectively. Assuming a single-chain Huang-Rhys parameter of unity,[6] the ratio is

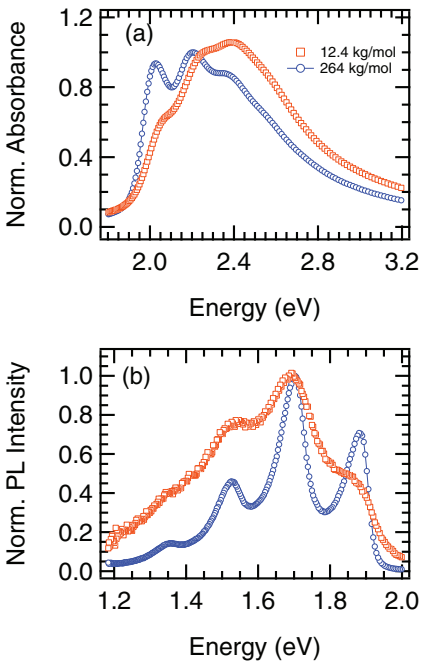

FIG. 1. (Color online) Absorption and photoluminescence spectra in thin films of neat P3HT of low (12.4 kg/mol; chain extended structure- red symbols) and high (264 kg/mol; entangled, semicrystalline morphology- blue symbols). (a) Normalized absorption spectra for these films at room temperature. (b) Normalized photoluminescence spectra measured at $T = 10$ K.

given by[5,6,27]

$$\frac{A_{0\text{-}0}}{A_{0\text{-}1}} \approx \left(\frac{1 - 0.24W/\hbar\omega_0}{1 + 0.073W/\hbar\omega_0}\right)^2, \quad (1)$$

where $\hbar\omega_0 = 180$ meV is the effective energy of the main intramolecular vibrational mode coupled to the electronic transition. Our optical absorption data presented in Fig. 1(a) thus suggests that W decreases significantly in high-M_w materials compared to P3HT of low M_w. We associate this noticeable variation in W between the two samples to conformational changes resulting from the significantly different average chain lengths associated with these two films. Excitonic coupling has been reported to vary inversely with conjugation length in P3HT,[4,37] consistent with theoretical predictions.[38–41] Similar trends have been reported in a series of chiral oligothiophenes endcapped with ethylene oxide side chains.[37]

The second important difference in the absorbance spectra of low- and high-M_w materials is the change in relative spectral weight at photon energies around 2.4 eV, which is higher for the sample of lower M_w. Absorbance in this high-energy region can be largely assigned to electronically uncoupled chromophores,[6,23] implying that the lower M_w sample is comprised of a higher fraction of photophysically uncoupled polymer chains.

Further information can be obtained from the corresponding PL spectra of the two low- and high-M_w samples, measured at 10 K [see Fig. 1(b)]. Specifically, we observe a 0-0 (1.88 eV)/0-1 (1.70 eV) PL ratio that is significantly larger in the P3HT film of higher M_w; we discuss this trend in more detail later in this section. In addition, we note that the

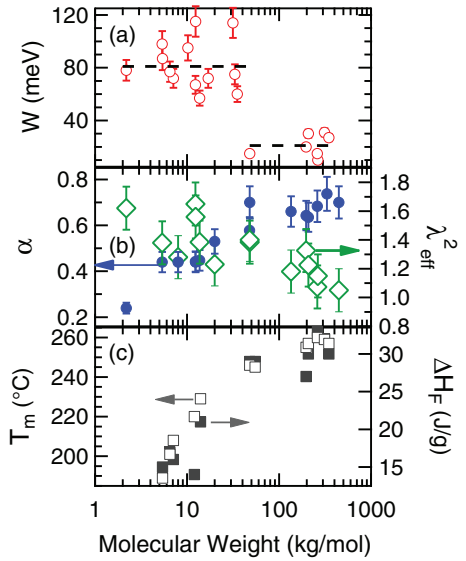

FIG. 2. (Color online) Dependence of spectroscopic and microstructural features and parameters from spectral analysis on molecular weight of neat P3HT architectures. (a) Free-exciton bandwidth W, derived from absorption spectra at room temperature. (b) Relative intensity of the 0-0 PL band α and effective Huang-Rhys parameter λ^2_{eff}, derived from photoluminescence spectra at 10 K. (c) Melting temperature T_{m} and enthalpy of fusion ΔH_{f}, derived from differential scanning calorimetry measurements.

0-2 (1.52 eV)/0-1 (1.70 eV) intensity ratio also depends on M_{w}; the smaller ratio for the higher-M_{w} samples indicating a *smaller* Huang-Rhys parameter. This is somewhat surprising as it is inconsistent with the weakly-coupled H-aggregate model,[23] which predicts that in the weak excitonic coupling regime the *relative* intensities of the 0-1, 0-2,... satellites should be independent of W (and disorder) and, hence, should resemble what is obtained for an isolated chromophore. Aggregation mainly influences the relative 0-0 peak intensity which depends entirely on the coherence of the emitting exciton, in marked contrast to the mainly incoherent origin of the vibronic satellites.

In order to examine these trends more quantitatively we measured absorption and PL spectra in a series of neat P3HT thin films using materials of M_{w} ranging from 2 to 347 kg/mol. We first plot W versus M_{w} [see Fig. 2(a)], derived from Eq. (1). For materials of $M_{\text{w}} < 50$ kg/mol, we deduce an average $W = 81 \pm 11$ meV, while for P3HT of higher M_{w}, we consistently derive an average W of 21 ± 2 meV. (In Supplemental Material[43] we show that the values of W increase by roughly 30% when evaluated using the HJ-aggregate model.) Tellingly, this transition of W is abrupt and occurs around $M_{\text{w}} \approx 50$ kg/mol, which is the molecular-weight region where the P3HT chains attain sufficient length to undergo entanglement, leading to a microstructural change from a paraffinic, chain extended phase to a two-phase morphology composed of interconnected crystalline and amorphous regions.[10,12,16,18,42] From the PL spectra of all the samples, we obtain the 0-0/0-1 intensity ratio and the *effective* Huang-Rhys parameter as a function of M_{w} via a fit with modified Franck-Condon model (see below) that takes into account the H-aggregate nature of the PL spectrum, namely, a symmetry-forbidden but disorder-allowed intensity of the 0-0 peak at 1.88 eV:[6]

$$I(\omega) \propto (\hbar\omega)^3 n^3(\omega) e^{-\lambda^2_{\text{eff}}} \left[\alpha \Gamma(\hbar\omega - E_0) + \sum_{m=1,2,\ldots} \frac{\lambda^{2m}_{\text{eff}}}{m!} \Gamma(\hbar\omega - E_0 + m\hbar\omega_0) \right], \quad (2)$$

where $n(\omega)$ is the refractive index of the film at the optical frequency ω, λ^2_{eff} is the effective Huang-Rhys parameter, E_0 is the energy of the origin of the vibronic progression, $\hbar\omega_0 = 180$ meV is the energy of the effective oscillator coupled to the electronic transition, and Γ is a Gaussian function that represents the inhomogeneously broadened spectral line of the vibronic replica in the progression. The parameter α thus quantifies the relative intensity of the origin of the vibronic progression (0-0), which is decoupled from the rest of the progression because it alone expresses the spatial coherence of the emitting Frenkel exciton within the H-aggregate model.[23] We display α and λ^2_{eff} as a function of M_{w} in Fig. 2(b). As the M_{w} of the P3HT films increases, we observe a strong increase in α from 0.24 to 0.74, correlated with a decrease of λ^2_{eff} from $\sim$1.5 to just over 1 for high-M_{w} samples. Note that for the analysis of the absorption spectrum reported in Fig. 2(a), we assumed $\lambda^2_{\text{eff}} = 1$. We also extracted values for W using λ^2_{eff} from the PL analysis in Fig. 1(b), using a more general expression reported elsewhere[28] (see Supplemental Material[43]), generalized for arbitrary HR factors. This increases W by $\sim$50%. However, we expect that λ^2_{eff} in the absorption spectrum is intermediate between 1 and that measured by PL since the distribution of chromophore configurations is larger in absorption. Therefore we choose to report W in Fig. 2(a) obtained by imposing $\lambda^2_{\text{eff}} = 1$.

The increase in α—the relative 0-0 intensity—can be accounted for in the H-aggregate model as a decrease in W, an increase in the energetic disorder magnitude (quantified by the width σ of a Gaussian distribution of site energies), a decrease in spatial correlation of site energies (β), or some combination of the above. Here, $\beta \equiv \exp(-1/l_0)$, where l_0 is the site-energy spatial correlation length in units of the interchain separation. (Note that β ranges from 0 to 1 as l_0 increases from 0 to infinity.) From the perturbative expression derived in Ref. 27 the scaling of the 0-0/0-1PL ratio with the parameters σ, β, and W is

$$\frac{I^{0\text{-}0}}{I^{0\text{-}1}} \sim \frac{(1-\beta)\sigma^2}{(1-\beta)W^2}, \quad (3)$$

which is strictly valid in the limit where $(1-\beta)\sigma \ll W \ll \hbar\omega_0$. Since the absorption and emission spectral linewidths are smaller in the higher-M_{w} films, the width of the disorder distribution is also smaller. A change in σ therefore cannot be responsible for the higher 0-0/0-1 ratio observed in the high-M_{w} materials. Moreover, increasing order is usually coincident with an increasing spatial correlation parameter β, which also serves to decrease the 0-0/0-1 ratio and hence contradicts what we observe. The full influence of spatial correlation will be explored in greater detail later in Sec. III B. (We find, in fact, that β increases for films prepared with higher-M_{w} P3HT.)

The data displayed in Fig. 2(a) shows, however, that W is significantly smaller for higher-M_w samples (consistent also with increasing order) and thus, according to the H-aggregate model, a reduction in W would account for the observed increase in the PL 0-0/0-1 ratio with M_w. Because of the large change in W in the two well-defined M_w regimes, we expect that this parameter will represent the dominant contribution to the trend in α. In the limit that W becomes negligible (i.e., in π stacks consisting of polymers with very long conjugation lengths[38–41]), the 0-0/0-1 line strength ratio is capped at the maximum value of value λ^2, the Huang-Rhys parameter representing a single chain in the π stack. Measurements of Kanemoto *et al.*[44] show that the single chain HR factor is approximately unity.

There is, however, evidence for the breakdown of the pure H-aggregate model in the recent literature. For instance, recent reports on P3HT whiskers (i.e., "nanofibers" grown from relatively high-molecular-weight materials from solution over time), have shown that the ratio of the 0-0 to 0-1 PL peaks can be as high as two at room temperature,[1] suggesting that the line strength can significantly exceed the aforementioned cap. Additional evidence for the breakdown of the H-aggregate model comes from the decrease of the 0-2/0-1 peak ratio in the PL spectrum of materials of increasing M_w reported in this paper [see Fig. 1(b)]. As mentioned in a prior work,[23] for the relatively weak values of W encountered in P3HT aggregates, the *relative* strengths of the side-band peaks (0-1, 0-2, etc.) in the PL spectrum very closely resemble the isolated molecular values; for example, the ratio of the 0-2 to 0-1 line strengths, $I^{0\text{-}2}/I^{0\text{-}1}$, remains steadfast at the value of $\lambda^2/2$, as determined from the Poissonian distribution for an isolated (single molecule) chain:

$$I^{0\text{-}n}_{\text{molec}} = \frac{\lambda^{2n} e^{-\lambda^2}}{n!}. \tag{4}$$

This relation is in disagreement with the data that is presented in Figs. 1(b) and 2(b), where we observe a significant decrease in the PL 0-2/0-1 ratio (decrease in λ^2_{eff}) with increasing M_w. More precisely, λ^2_{eff} decreases from approximately 1.3–1.6 for P3HT of low M_w to 1.0–1.1 for materials of high M_w. The apparent failure of the H-aggregate model, which assumes that a polymer chain has a unique HR factor independent of M_w, is due to its assumption that a single chain can be modeled as a two-level chromophore with displaced harmonic nuclear potentials characterized by a unique HR factor λ^2. This simple description assumes that the Born-Oppenheimer approximation is valid for a single chain and ignores exciton motion and nonadiabatic coupling to vibrations within a given chain. The consequences of intrachain exciton vibrational coupling were examined in Ref. 35, where a single conjugated polymer chain was modeled as a one-dimensional Wannier exciton coupled vibronically to the main symmetric vinyl-stretching mode. The electron and hole transfer integrals between neighboring unit cells were taken to have the same sign, consistent with what is normally assumed for conjugated polymer chains, and reflective of a direct band gap semiconductor. The ensuing photophysical properties of such "quantum wires" were found to be remarkably similar to linear J aggregates.[45] In Ref. 35, it was shown that the 0-0/0-1 line strength ratio in the PL spectrum of the single chain increases with intrachain exciton bandwidth—as expected for a J aggregate–while the 0-2/0-1 ratio decreases. The behavior can be crudely described as a decrease in the effective single chain Huang-Rhys factor with increasing exciton coupling, although the relative intensities are generally not Poissonian. An approximate description of this behavior in the adiabatic limit was provided by Chen and coworkers for a Frenkel chain,[46] as well as Cornil *et al.* for a polymer chain using quantum chemically derived adiabatic ground- and excited-state potentials.[47]

We therefore attribute the decrease in λ^2_{eff} that we observe in the P3HT samples of increasing M_w to an *increase* in the intrachain exciton bandwidth. This strongly suggests that in these high-M_w P3HT architectures, the macromolecules are of reduced torsional disorder. Such a transition to a more planar structure in samples of higher molecular weight would be in agreement with some of our thermal analysis data: indeed, we observe an increase in both the melting temperature T_m (which is directly correlated with the lamellar crystal thickness) and the enthalpy of fusion ΔH_f (which is directly correlated with the degree of crystallinity, see Koch *et al.*,[16] and references therein).

Further support for high-M_w P3HT structures being of higher torsional order (i.e more pronounced planarization of the polymer backbones) can be evoked from the ratio of the PL decay at 1.90 and 1.77 eV [see Fig. 3(c)]. We observe that in the low-M_w regime, the relaxation of the normalized ratio of intensities at these two photon energies is more significant than for high-M_w material. In fact, Parkinson *et al.* have reported that vibrational relaxation from a low-symmetry to a high-symmetry ordered state, characteristic of torsional

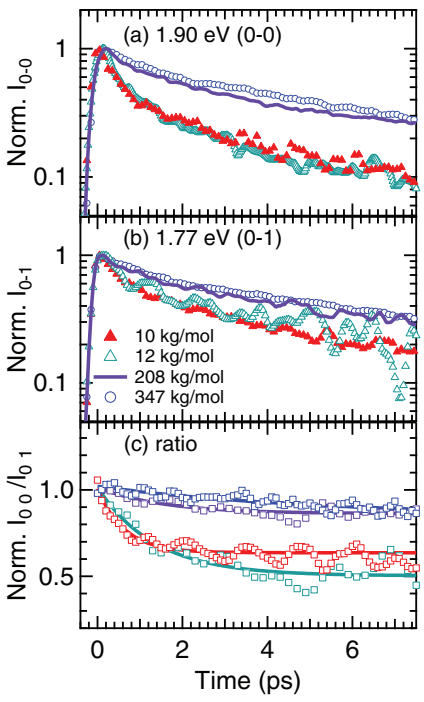

FIG. 3. (Color online) Time-resolved photoluminescence intensity measured at room temperature for various neat P3HT films, measured at photon energy of 1.90 eV (a) and 1.77 eV (b). The normalized ratio $I^{0\text{-}0}/I^{0\text{-}1}$ is plotted in (c).

planarization along the polymer backbone upon optical excitation, results in a dynamic decrease of the relative 0-0 PL intensity on a time scale ∼13 ps.[48] Such effect has also been observed by Banerji *et al.* on time scales >1 ps.[49] Moreover, recent broadband transient spectroscopy measurements have revealed signatures of both small-scale (<1 ps) and large-scale (>1 ps) planarization of P3HT thiophene units after excitation.[50] In other materials, such as PPV oligomers, the degree of torsional angle of the backbone is found to correlate with an increase of the oscillator strength for the 0-0 transition in comparison to the rest of the vibronic replicas.[51] This is consistent with higher initial torsional order in the high-M_w regime, which influences W and consequently α, the relative intensity of the 0-0 peak in PL. From this observation, we support our conjecture that the decrease in λ_{eff}^2 with increasing M_w is primarily due to an increase in intrachain exciton bandwidth resulting from a reduction in torsional disorder in high-M_w aggregates.

B. HJ-aggregate model

In order to obtain a more detailed knowledge about the relationship between exciton signatures and solid-state microstructure and macromolecular chain conformation and to explore the effect of intrachain exciton bandwidth on λ_{eff}^2 quantitatively, we generalize the HJ-aggregate model introduced in Ref. 36 to include disorder. In the HJ-aggregate model, excitons are free to navigate across chains in the π stack, as in the original H-aggregate model, but also *within* chains. Intrachain excitons are generally of the Wannier-Mott type in which electrons and holes are bound across more than one site with a characteristic Bohr radius. Hence, within a π stack of such chains, the exciton is delocalized over two dimensions; along the polymer backbone as well as along the stacking axis. Because the Wannier-Mott excitons in one dimension lead to J-aggregate photophysics,[35] the aggregate can be understood as J-like along the backbone dimension and H-like along the stacking direction, allowing for interesting hybrid H-J photophysical properties. If disorder is absent, as was the case treated in Ref. 36, the high symmetry dictates that no 0-0 emission can occur at low temperatures—a classic signature of H aggregates. Increasing temperature leads to interesting effects, for example, a transition from H- to J-aggregate behavior with increasing temperature has been predicted.[36] Similar effects are expected when correlated disorder (quantified by σ and β) is included.

In this section, we show that the intrachain and interchain exciton bandwidths *corresponding to the emitting aggregate species* can be determined entirely from an analysis of the PL vibronic progression; in particular from the 0-2/0-1 and 0-0/0-1 ratios. This has an advantage over some prior analyses based on the H-aggregate model where the (interchain) exciton bandwidth was extracted from the 0-0/0-1 absorption spectral ratio, which is characteristic of the *absorbing* species. In polymer films, absorption and emission very likely take place from configurationally inequivalent species, as the significant disorder inherent to such films enhances spectral diffusion away from the primary absorbers.

In conjugated polymer chains, the ratio of the 0-0 and 0-1 oscillator strengths in the absorption spectrum can be quite large—almost a factor of ten in the isolated and practically disorder-free polydiacetylene (PDA) chains,[34] for example—and is a direct measure of the strength of the intrachain exciton coupling. In modeling a single P3HT chain, we assume weaker intrachain coupling than in PDA because the 0-0/0-1 absorption peak ratio in P3HT (in solution or solid phase) has never been observed to increase much beyond unity. In the weak coupling limit, second-order perturbation theory shows that transport along the chain occurs via virtual two-step electron-hole (or vice versa) events involving Frenkel-like excitations within a single monomer unit (i.e., thiophene unit).[36] Such a chain can be described with a Frenkel-like Holstein Hamiltonian in which the (through-bond) exciton coupling between adjacent thiophene units is given by

$$J_{\text{intra}} = -\frac{2t_e t_h}{U - V_1}. \tag{5}$$

Equation (5) contains the product of electron (t_e) and hole (t_h) transfer integrals connecting neighboring thiophene LUMO's and HOMO's, respectively. $U - V_1$ is the stabilization of the neutral Frenkel-like exciton relative to the nearest-neighbor charge-separated state. Note that the single-chain physics is invariant to a sign change in *both* t_e and t_h. In addition to an effective coupling between adjacent thiophene units, there is also a second-order energy (red) shift, given by

$$\Delta_{\text{intra}} = -\frac{2\left(t_e^2 + t_h^2\right)}{U - V_1} \tag{6}$$

due to virtual two-step transfer where, for example, an electron (or hole) moves to a neighbor and then returns to the parent thiophene ring.

As in Ref. 36, we assume equivalent electron and hole transfer integrals, and introduce t such that $t \equiv t_e = t_h$. Having $t_e = t_h$ is consistent with a direct band-gap semiconductor. Within this approximation, Eq. (5) leads to

$$J_{\text{intra}} = -2t^2/(U - V_1), \tag{7a}$$

where the negative sign on the right-hand side ensures J-aggregate-like behavior. Inserting $t_e = t_h$ in Eq. (6) leads to a simple relation between the red shift and J_{intra},

$$\Delta_{\text{intra}} = 2J_{\text{intra}}. \tag{7b}$$

Since the P3HT chains are generally torsionally disordered, we consider t (and J_{intra}) to be an *effective* coupling, smaller than the larger intrinsic coupling found in the "perfect" polydiacetylene chains.[35]

Within the space of a single electronic excitation (one electron and one hole), the single-chain effective Hamiltonian representing the sth disorder-free P3HT chain is therefore given by

$$\begin{aligned}\hat{H}_{s,\text{chain}} = {} & \varepsilon_1 + \Delta_{\text{intra}} + \hbar\omega_0 \sum_n b_{n,s}^\dagger b_{n,s} \\ & + \hbar\omega_0 \sum_n \left\{\lambda_0 (b_{n,s}^\dagger + b_{n,s}) + \lambda_0^2\right\} |n,s\rangle\langle n,s| \\ & + J_{\text{intra}} \sum_n \{|n,s\rangle\langle n+1,s| + |n+1,s\rangle\langle n,s|\}. \end{aligned} \tag{8}$$

$|n,s\rangle$ represents an electron-hole (Frenkel-like) excitation ("S_1") on the nth thiophene unit of the sth chain with energy

ε_1. The operator $b^\dagger_{n,s}(b_{n,s})$ creates (destroys) a vibrational quantum of energy, $\hbar\omega_0$, (corresponding to the symmetric ring-stretching mode) in the ground state nuclear potential well (the "S_0" potential) associated with a neutral "ground state" repeat unit at the nth site on chain s. (Such a unit contains no electrons and holes). The quantity λ_0^2 is the Huang-Rhys factor for an *individual* thiophene unit and is set to 2, which we calculate for uncoupled thiophene monomers by means of time-dependent density functional theory (see Supplemental Material[43]).

Energetic site disorder within the sth chain is represented by the Hamiltonian

$$H_{s,\mathrm{dis}} = \sum_n \Delta_{n,s}|n,s\rangle\langle n,s|, \tag{9}$$

where $\Delta_{n,s}$ is the transition frequency detuning of the nth thiophene unit on the sth chain. In what follows, we take the detunings, $\Delta_{n,s}$, to be Gaussian random variables distributed with probability

$$P(\Delta_{n,s}) = \frac{1}{\sqrt{\pi}\sigma} e^{-\Delta^2_{n,s}/\sigma^2}.$$

Here, 2σ is the full width of the distribution at $1/e$ of the maximum. The spatial correlation length, l_0, is defined through an exponential drop in the intersite correlation function,[23,52]

$$\langle \Delta_{n,s}\Delta_{n',s'}\rangle = (\sigma^2/2)\exp[-\sqrt{(n-n')^2+(s-s')^2}/l_0].$$

Here, l_0 is in units of d, where $d \approx 4$ Å is the (approximate) distance between nearest-neighbor chains as well as the distance between nearest-neighbor thiophene units within a given chain. The monomer units in a π stack therefore constitute a square lattice with a spatial correlation *radius* given by l_0. As before [see discussion following Eq. (3)], the correlation parameter β is associated with l_0 through $\beta = \exp(-1/l_0)$.[52] In a more sophisticated treatment, the interchain and intrachain disorder included in Eq. (9) can be distinguished by introducing spatial correlation lengths along and across the polymer backbone. However, as of the time of this writing, we have no clear data to suggest what the anisotropy in the l_0 values might be. Although increasing the value of l_0 along a particular direction would enhance the coherence length along that direction, the effect is not large (see Fig. 9, which shows a remarkable stability of the coherence length to changes in the correlation length). Finally, we emphasize that the torsional disorder is also reflected in the *mean* intrachain coupling J_{intra}. In principle, J_{intra} should be correlated to l_0. Here, we treat them as independent variables but look for consistency in our final results (see below).

The complete Hamiltonian for the π stack including disorder reads

$$H_{\pi\,\mathrm{stack}} = \sum_s (\hat{H}_{s,\mathrm{chain}} + H_{s,\mathrm{dis}}) + \sum_s \sum_n J_{\mathrm{inter}}\{|n,s\rangle\langle n,s+1| + |n,s+1\rangle\langle n,s|\}, \tag{10}$$

where the through-space, interchain coupling J_{inter} is limited to adjacent (same n) thiophene units on neighboring chains.[36] Note that the H-aggregate model is recovered in the limit that J_{intra} is set to zero.

In order to derive the mean intramolecular coupling J_{intra}, from the measured PL spectra, we first introduce the effective HR factor, defined as

$$\lambda^2_{\mathrm{eff}} \equiv 2\frac{I^{0\text{-}2}_{\mathrm{PL}}}{I^{0\text{-}1}_{\mathrm{PL}}}, \tag{11}$$

where $I^{0\text{-}\nu}_{\mathrm{PL}}$ is the line strength corresponding to the 0-ν transition. As we will show, the effective HR factor defined by Eq. (11) is far more sensitive to the *intrachain* exciton bandwidth than the interchain exciton bandwidth, thereby providing an effective measure of the former. (By contrast, the ratio $I^{0\text{-}0}_{\mathrm{PL}}/I^{0\text{-}1}_{\mathrm{PL}}$ responds to the exciton *coherence number* due to the competition between the intrachain and interchain exciton coupling.)

In the limit of just a single, site-disordered chain with $J_{\mathrm{intra}} = 0$ (i.e., a linear array of noninteracting thiophene units) λ^2_{eff} reduces to the monomeric HR factor λ_0^2, (which we take to be two), as can be appreciated from the Poissonian distribution in Eq. (2). Increasing $|J_{\mathrm{intra}}|$ enhances the J-aggregate behavior: the 0-0/0-1 line strength ratio in PL spectrum increases in response to the increasing exciton coherence length, while the 0-2/0-1 ratio *decreases*. The overall result is a decrease in the effective HR factor. The effect is shown in Fig. 4 for several values of the disorder correlation parameter, β, with the value of σ taken from the absorption spectral linewidths of the high-M_{w} films when fitted to a Gaussian line shape. (σ is the half-width at $1/e$ of the maximum). From Fig. 1(a), we have $\sigma = 0.6\omega_0$ and $0.54\omega_0$, for the low- and high-M_{w} samples, respectively. Figure 4 shows that λ^2_{eff} decreases markedly with increasing intrachain coupling, as expected for J aggregates.

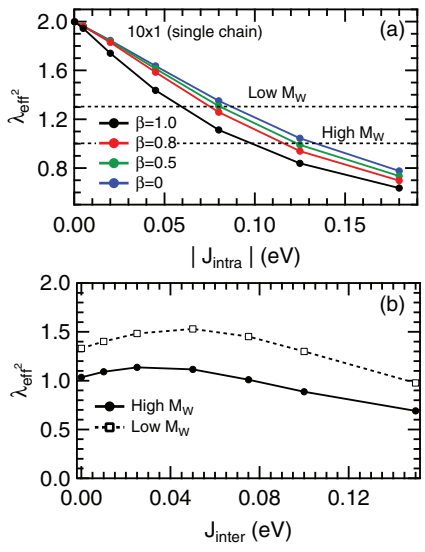

FIG. 4. (Color online) Calculated effective Huang-Rhys parameter as a function of intramolecular and intermolecular coupling. (a) λ^2_{eff} as a function of $|J_{\mathrm{intra}}|$ for a single polymer chain containing 10 thiophene units with $\lambda_0^2 = 2$. Several disorder parameters β are shown, with $\sigma = 0.54\hbar\omega_0$. (b) λ^2_{eff} as a function of interchain coupling for 10 by 6 aggregates of high- and low-molecular-weight chains with $\beta = 0.6$.

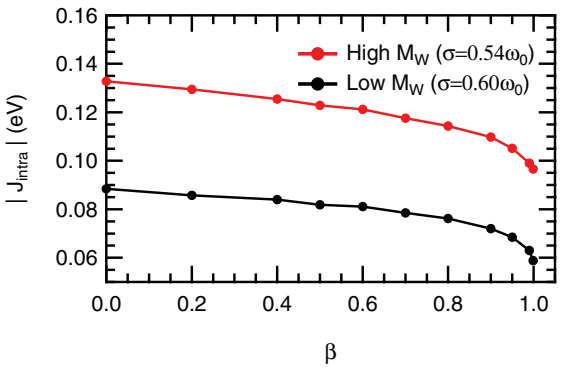

FIG. 5. (Color online) Values of (β, J_{intra}) for which the effective HR factor, λ^2_{eff} is constant at 1.0 and 1.3 for single (isolated) chains of low and high M_{w}, respectively. Each chain contains ten thiophene rings (sufficient for convergence) and the ensemble average included 10^4 configurations. For the low (high) M_{w} chains, the value of σ is $0.60\omega_0$ ($0.54\ \omega_0$) as determined from the absorption spectral linewidths.

After removing the cubic frequency dependence and the index of refraction dependence from the measured PL spectra in Fig. 1(b), the experimentally obtained values of λ^2_{eff} were determined to be approximately 1.5 for the low-M_{w} materials and 1.1 for P3HT of high M_{w}. However, in our modeling of a single chain, we take the slightly smaller values of 1.3 and 1.0, for the low- and high-M_{w} films, respectively, since, as will be shown shortly, the values increase slightly when interchain effects are included. Figure 4 shows that λ^2_{eff} attains the value of near unity observed in films of P3HT of high M_{w} when $|J_{\text{intra}}|$ is in the range 0.1–0.15 eV, while the value observed for low-M_{w} material is consistent with values of $|J_{\text{intra}}|$, some 30% smaller.

Figure 4(b) shows how λ^2_{eff} varies with *inter*chain coupling, J_{inter}, for the two values of $|J_{\text{intra}}|$, which reproduce the measured effective HR factors for low- and high-M_{w} materials for a representative value of $\beta = 0.6$. (Other values of β give qualitatively similar behavior.) The dependence on J_{inter} is much weaker than the dependence on $|J_{\text{intra}}|$, although there is a slight but significant initial rise in λ^2_{eff} with J_{inter}, followed by a peak and subsequent demise. The weak dependence of λ^2_{eff} on interchain interactions was shown analytically using the H-aggregate model in Ref. 27 and demonstrated numerically in Ref. 23. The weak dependence is therefore due to the positive sign of the interchain coupling.

Figures 4(a) and 4(b) also show that λ^2_{eff} serves as an effective probe of the intrachain exciton bandwidth and disorder parameter β. Armed with the measured value of λ^2_{eff} for the low- and high-M_{w} films (1.3 and 1.0, respectively), we then determined the points (β, J_{intra}), which reproduce the measured λ^2_{eff} in an ensemble of disordered *single* chains containing 10 thiophene units each. (Ten units are enough to ensure convergence to the polymer limit.) The results are plotted in Fig. 5 for both low- and high-M_{w} films. Our results show that generally slightly larger values of J_{intra} are required when disorder is increased (β reduced) and that the low-M_{w} films have uniformly lower values of $|J_{\text{intra}}|$ than films prepared with high-M_{w} materials, consistent with increased torsional disorder in the low-M_{w} films.

We next turn to the effects of interchain coupling. To this end, we first took representative points on the curves in Fig. 5 and varied J_{inter} for each one until the calculated 0-0/0-1 ratio in the PL spectrum matched the measured values. Unlike λ^2_{eff}, the 0-0/0-1 PL ratio is extremely sensitive to exciton spatial coherence[23,24] and depends in a complex way on the exciton coupling along and across chains.[36] For the two featured P3HTs, of low (12.4 kg/mol) and high (264 kg/mol) M_{w}, the 0-0/0-1 ratios were approximately 0.3 and 0.55, respectively, after removal of the cubic frequency dependence and index of refraction dependence. The values of J_{inter}, which maintain the measured 0-0/0-1 PL ratio, are shown in Table I. Ideally, if interchain interactions had no impact on λ^2_{eff}, all of the "triple points" (β, J_{intra}, J_{inter}) in Table I would reproduce both the measured 0-2/0-1 and 0-0/0-1 ratios in the PL spectrum. Table I shows that λ^2_{eff} increases with the disorder as anticipated from Fig. 4(b). The increase, however, is quite modest and within the experimental error bars for both low- and high-M_{w} samples (1.5 and 1.1, respectively) when $\beta > 0.5$.

Table I shows that as disorder increases (and l_0 diminishes) both $|J_{\text{intra}}|$ and J_{inter} also increase in order to keep the 0-0/0-1 ratio constant. J_{inter} increases by more than an order of magnitude over the full disorder range reported in the Table, far greater than the modest increase of only 30% for $|J_{\text{intra}}|$. The main reason for the large increase in J_{inter} is to counter

TABLE I. Values of β and $|J_{\text{intra}}|$ from Fig. 5 along with values of J_{inter}, which maintain the 0-0/0-1 PL ratio at 0.56 in films of high-M_{w} P3HT and 0.30 in low-M_{w} films.

		High M_{w}				Low M_{w}			
	l_0	$\lvert J_{\text{intra}}\rvert$ (eV)	J_{inter} (eV)	$I^{0\text{-}0}/I^{0\text{-}1}$	λ^2_{eff}	$\lvert J_{\text{intra}}\rvert$ (eV)	J_{inter} (eV)	$I^{0\text{-}0}/I^{0\text{-}1}$	λ^2_{eff}
0	0.0	0.133	0.045	0.56	1.24	0.088	0.085	0.3	1.62
0.2	0.6	0.129	0.041	0.56	1.21	0.086	0.078	0.3	1.60
0.4	1.1	0.126	0.035	0.56	1.18	0.084	0.069	0.3	1.56
0.5	1.4	0.123	0.032	0.56	1.17	0.082	0.065	0.3	1.54
0.6	2.0	0.121	0.030	0.56	1.14	0.081	0.061	0.3	1.51
0.7	2.8	0.117	0.028	0.56	1.13	0.078	0.055	0.3	1.50
0.8	4.5	0.114	0.024	0.56	1.10	0.076	0.048	0.3	1.46
0.9	9.5	0.110	0.020	0.56	1.07	0.072	0.039	0.3	1.42
0.95	19.5	0.105	0.015	0.56	1.05	0.068	0.030	0.3	1.39
0.99	99.5	0.099	0.008	0.55	1.03	0.063	0.016	0.3	1.34
0.999	999.5	0.097	0.003	0.57	1.01	0.058	0.006	0.3	1.32

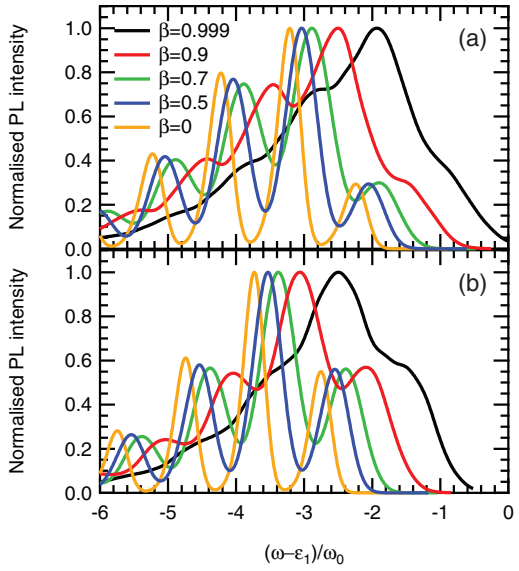

FIG. 6. (Color online) Calculated PL spectra for selected triple points from Table I for materials of molecular weights in the low- (a) and high-M_w (b) limits. Ensemble averaging includes 10^4 configurations of disorder ($T = 10$ K).

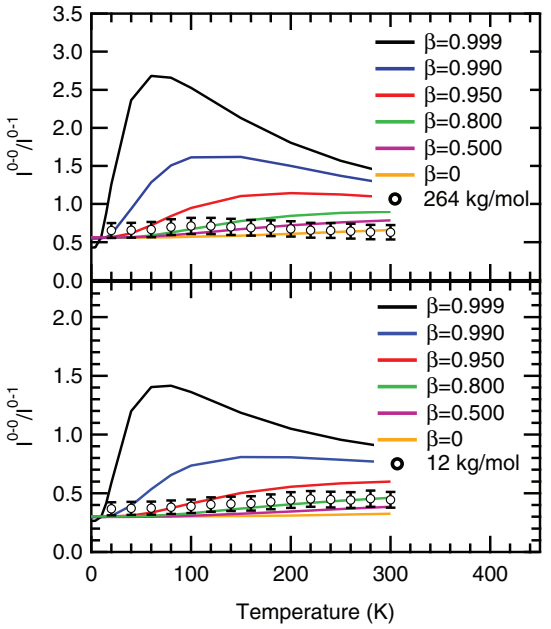

FIG. 7. (Color online) The 0-0/0-1 PL ratio as a function of temperature for selected triple points (see Table I) for P3HT thin films of high and low M_w. Also shown is the experimental data for the 447 kg/mol film (a) and 8 kg/mol (b) at $T = 10$ K.

the enhancement of the 0-0/0-1 ratio due to the symmetry breaking induced by increasing disorder.

Calculated PL spectra for selected triple points are shown in Fig. 6, assuming that emission takes place from a Boltzmann distribution of band-bottom excitons, i.e., after relaxation has taken place.[36] The evaluation of the PL spectrum from a thermal population of exciton emitters is outlined in Ref. 36. Here we perform an additional averaging over many (10^4) realizations of spatially-correlated disorder consistent with (σ, l_0). Figure 6 shows that the 0-0/0-1 ratio is constant throughout the series, whereas the 0-2/0-1 ratio exhibits the aforementioned slight rise as disorder increases. The linewidths significantly redshift and narrow with increasing disorder due to a statistical effect discussed in detail in Ref. 23. Essentially, the probability of finding a low-energy emitting trap increases when the spatial correlation length l_0 is smaller (β smaller). Comparison with the experimental linewidths for films of low- and high- M_w P3HT (see Fig. 1) suggests that β is in the range, $0.5 < \beta < 0.9$, equivalent to a correlation length in the range, $1 < l_0 < 10$. The measured spectra of Fig. 1(b) further show that the 0-0 transition energies of the low- and high-M_w samples are approximately the same. To obtain spectrally-aligned 0-0 peaks in the PL spectra in Fig. 6 requires β to be larger in the higher-M_w samples, for example, when $\beta = 0.9$ in the high-M_w films and $\beta = 0.5$ in the low-M_w films the positions of the 0-0 peaks are roughly the same. This is consistent with films of P3HT of low M_w featuring a higher degree of energetic disorder.

We now turn to the temperature dependence of the 0-0/0-1 ratio. The measured temperature dependence is shown in Fig. 7 for P3HT of low (12 kg/mol) and high (264 kg/mol) M_w, alongside the calculated temperature dependence for the selected triple points from Table I. The temperature dependence was evaluated by performing a Boltzmann average over emitting excitons for each disordered chain in the ensemble. When disorder within each chain is minimal ($\beta > 0.95$) the form of the calculated temperature dependence is similar to what was derived in Ref. 36 in the limit of no disorder. The initial increase with T is a result of increasing population of the optically allowed higher energy exciton, as occurs in interchain H aggregates. The peak occurs when kT is approximately equal to the interchain splitting, and the subsequent demise is the expected behavior for J aggregates. When disorder increases, the temperature dependence flattens out considerably and better agrees with the measured trend, as depicted in Fig. 7. Comparison of calculated and measured data shows that the spatial correlation parameter β is most likely less than approximately 0.7 in both low- and high-molecular-weight samples.

C. Exciton coherence

In what follows, we will consider exciton coherence within the two-dimensional P3HT π stacks. We are primarily interested in the exciton coherence corresponding to the thermally relaxed distribution of excitons, which gives rise to the steady-state PL spectrum. The corresponding coherence length is limited by the localizing influences of disorder, vibronic coupling and increasing temperature. We are not concerned with the early-time evolution of exciton coherence during relaxation/thermalization, which is driven by inhomogeneous and homogeneous dephasing. The latter is due to interactions between the π stack and the surrounding bath, arising, for example, from lattice phonons. Due to the inherent anisotropy of exciton coupling in P3HT π stacks, we expect the coherence length along the polymer backbone, $L_\parallel$, and along the stacking axis, $L_\perp$, to differ. Moreover, as we will show, both coherence lengths depend on the polymer molecular weight.

For a thermal distribution of low-energy excitons responsible for emission and transport, the ensemble-averaged coherence function is given by[23,53]

$$\bar{C}(\boldsymbol{r}) \equiv \left\langle \langle \psi^{(\mathrm{em})} | \sum_{\boldsymbol{R}} B^{\dagger}_{\boldsymbol{R}} B_{\boldsymbol{R}+\boldsymbol{r}} | \psi^{(\mathrm{em})} \rangle \right\rangle_{C,T}, \qquad (12)$$

where $B^{\dagger}_{\boldsymbol{R}} \equiv |\boldsymbol{R};\mathrm{vac}\rangle\langle g;\mathrm{vac}|$ creates an exciton at the monomer site $\boldsymbol{R}$ with no vibrational quanta (vac) relative to the ground state unshifted potential well. Here, the vector $\boldsymbol{R} = (n,s)$ locates the nth monomer repeat unit on the sth chain. $\langle\cdots\rangle_{C,T}$ represents a dual configurational and thermal average, the former taking place over the various realizations of site-energy disorder and the latter taking place over a Boltzmann distribution of emitting excitons within each realization of disorder. The $\boldsymbol{r}$-dependent coherence in Eq. (12) is similar to that used by Mukamel and coworkers[22,54,55] and Kuhn and Sundstrom.[21]

Coherence in P3HT using the H-aggregate model was investigated in Ref. 23. As the H-aggregate model is one-dimensional, only the coherence along the π-stacking direction was considered. It was shown that in such aggregates the coherence function oscillates along the aggregate axis, changing sign as $(-1)^n$, where n labels the nth polymer in the stack. The oscillation reflects the dominant admixture of the high wave vector ($k = \pi$) exciton in the band-bottom excitons, as is characteristic of disordered H aggregates.[23] By contrast, in linear J aggregates, the coherence function is nodeless, reflecting the dominant admixture of the $k = 0$ exciton in the band-bottom excitons.[44]

Figure 8 shows the two-dimensional coherence functions for films of high- and low-M_{w} P3HT evaluated from Eq. (12) using $\beta = 0.6$, with the coupling parameters taken from Table I. Interestingly, the coherence function contains properties of H and J aggregation: the oscillations along the π-stacking direction results from the positive sign of the interchain coupling and signals H aggregation, while the uniform phase of $\bar{C}(\boldsymbol{r})$ along the chain direction results from the negative sign of the intrachain interactions and signals J aggregation. Figure 8 shows that the coherence has greater extent along the polymer chain for P3HT of higher M_{w} where the intrachain coupling is about 50% larger than in the low-M_{w} materials (see Table I). Although not as obvious, the opposite holds for the coherence along the π-stacking axis; it has a greater extent for films prepared with low-M_{w} materials, where the interchain coupling is twice as large compared with P3HT of higher M_{w} (see Table I). Figure 8 also shows that the coherence function is more anisotropic in the higher-M_{w} films.

Based on the coherence function in Fig. 8, one can approximate the total number of monomeric units, N_{coh}, within the coherence "area" defined by the spatial extent of the *envelope* of the coherence function. A more quantitative evaluation of N_{coh} follows from the simple relation,[23,44]

$$N_{\mathrm{coh}} = \bar{C}(0)^{-1} \sum_{\boldsymbol{r}} |\bar{C}(\boldsymbol{r})|, \qquad (13)$$

where the dimensionless vector $\boldsymbol{r}$ runs over all monomer-monomer separation vectors within the π stack. The absolute value dependence on $\bar{C}(\boldsymbol{r})$ eliminates the phase oscillations, since N_{coh} depends on the envelope of $\bar{C}(\boldsymbol{r})$. For example, in a linear H aggregate that is fully coherent (so that $N_{\mathrm{coh}} = N$), the oscillations present in $\bar{C}(\boldsymbol{r})$ lead to complete destructive interference in the sum, $\sum_{\boldsymbol{r}} \bar{C}(\boldsymbol{r})$, making it necessary to instead sum over $|\bar{C}(\boldsymbol{r})|$ in order to determine N_{coh}. Indeed, the sum in Eq. (13) gives the correct result, $N_{\mathrm{coh}} = N$ (assuming, as we are, periodic boundary conditions).

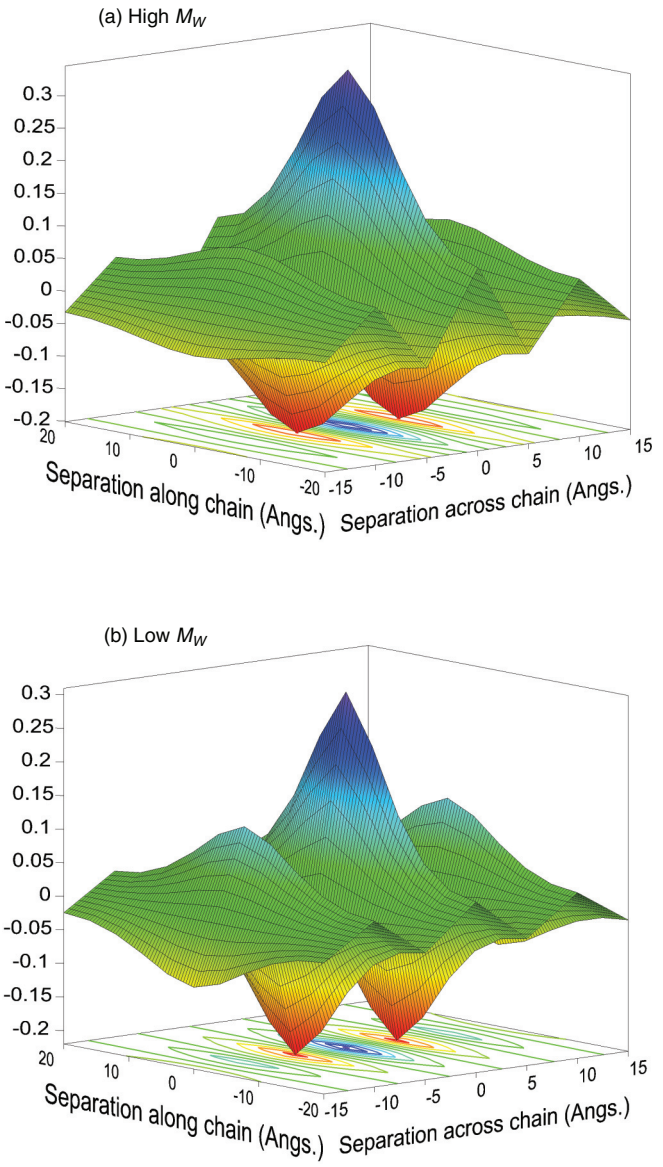

FIG. 8. (Color online) Coherence function from Eq. (13) for low- and high-M_{w} samples and $\beta = 0.6$. Calculations are conducted on 6 by 10 aggregates (six chains each containing ten thiophene rings).

The coherence number defined in Eq. (13) has the correct limiting behaviors, ranging from unity when the coherence function is fully localized [$\bar{C}(\boldsymbol{r}) = \bar{C}(0)\delta_{\boldsymbol{r},0}$] to N when the coherence is spread over the entire aggregate. N_{coh} differs from previously defined measures of exciton coherence sizes,[20] such as the inverse participation ratio. The advantage of our definition is the simple and direct relationship N_{coh} has to the exciton superradiant enhancement and, more importantly, to the 0-0/0-1 PL ratio in J aggregates (see below).

The coherence number N_{coh} depends mainly on the nature of disorder (σ, l_0) as well as the temperature. Generally,

increasing disorder and/or temperature localizes excitations and reduces N_{coh} as demonstrated in detail in Refs. 23 and 44 for H and J aggregates, respectively. Vibronic coupling is also important since it weakens the excitonic coupling, thereby allowing the disorder-induced localization to be more effective. Using Eq. (13) we find that N_{coh} is $\approx$16 for the low-M_{w} P3HT films of Fig. 8(b) and $\approx$18 for the high-M_{w} films of P3HT of Fig. 8(a). Since the temperature is low ($T = 10$ K), it is disorder that is mainly responsible for localizing exciton coherence in both P3HT of low and high M_{w}.

In the π stack, one can also define the coherence *lengths* along the polymer chain direction ($L_{\parallel}$) and along the π-stacking axis ($L_{\perp}$) from the coherence function via

$$L_{\parallel} \equiv d_{\parallel} \left\{ \bar{C}(0)^{-1} \sum_{\boldsymbol{r}\in\mathrm{chain}} |\bar{\boldsymbol{C}}(\boldsymbol{r})| - 1 \right\}, \tag{14a}$$

$$L_{\perp} \equiv d_{\perp} \left\{ \bar{C}(0)^{-1} \sum_{\substack{r\in\mathrm{chain} \\ \mathrm{normal}}} |\bar{C}(\boldsymbol{r})| - 1 \right\}, \tag{14b}$$

where $d_{\parallel}$ ($d_{\perp}$) is the nearest-neighbor distance between two adjacent thiophene units within a chain (on neighboring chains). As stated earlier, we take both distances to be 4.0 Å in our calculations. Note that the term $\boldsymbol{r} = 0$ is included in both sums of Eqs. (14a) and (14b). Also note that in the limit of strong localization where $\bar{C}(\boldsymbol{r}) = \bar{C}(0)\delta_{\boldsymbol{r},0}$ the coherence lengths properly tend to zero.

Based on the coherence functions in Fig. 8 and the use of Eqs. (14a) and (14b), the coherence lengths along the polymer backbone and along the stacking axis are calculated in a 6 by 10 aggregate (6 chains with 10 thiophene units per chain). Figure 9 shows the coherence lengths of the low and high-M_{w} materials for each of the triple points of Table I. The coherence size is remarkably stable throughout the range from $\beta = 0$ to 0.95, corresponding to the spatial correlation length ranging from $l_0 = 0$ to 20 thiophene units. The coherence length begins to significantly increase when l_0 exceeds the chain length (10 units) used in the calculation; we therefore suspect that using larger chains in our calculations would lead to an increase

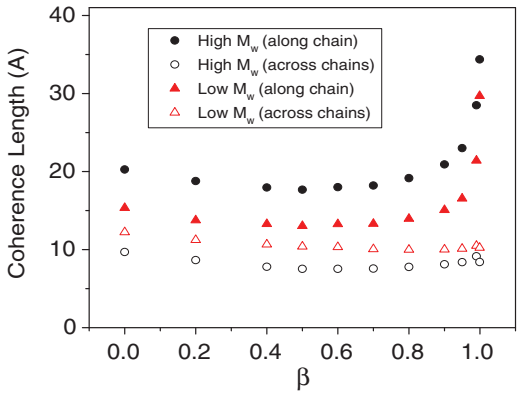

FIG. 9. (Color online) Coherence size defined in Eq. (11) as a function of disorder parameter β for P3HT films of low and high M_{w} at $T = 10$ K. Each point corresponds to triple point of Table I. Calculations are conducted on 6 by 10 aggregates (six chains each containing ten thiophene rings).

in the range of l_0 over which the coherence lengths remain approximately constant. When $\beta = 1$, each repeat unit in a given aggregate has essentially the same transition frequency, i.e., the intra-aggregate disorder is zero. Considering the 6 by 10 aggregates used on our calculations, the coherence length along the chain approaches $9d = 36$ Å, as is observed in Fig. 9. The coherence length across the chains should approach $5d = 20$ Å, however, in this limit, the small interchain interaction is of the order of kT at $T = 10$ K ($J_{\mathrm{inter}} = 0.003$ eV from Table I) so that the thermally induced localization remains significant.

From Fig. 9, the coherence length along the chain for P3HT of high M_{w} is about 18 Å (maintaining $\beta = 0.6$), which corresponds to slightly greater than four thiophene units. The coherence length drops to about 7.5 Å across chains. In materials of low M_{w}, the coherence is more isotropic; the coherence length along the chain is about 25% smaller than for high-M_{w} P3HT, although the coherence length across chains is significantly higher, approximately 10 Å, which is only slightly smaller than the value of $\approx$12 Å obtained using the H-aggregate model in Ref. 23. The greater coherence length along the chain for P3HT of high M_{w} is consistent with reduced torsional disorder, while the larger coherence length across chains for materials of low M_{w} arises mainly from the much higher interchain interactions (J_{inter}) within the π stacks of these materials (see Table I), possibly due to the higher torsional disorder in such structures, e.g., induced through end-group effects.

Relationship between N_{coh} and the PL line shape

We have written extensively on the uniquely coherent nature of the 0-0 peak within the PL vibronic progression.[5,24,44] For any aggregate type (H and J), the dimensionless 0-0 line strength is directly related to the averaged coherence function through

$$I_{\mathrm{PL}}^{0\text{-}0} = \sum_{\boldsymbol{r}} \bar{C}(\boldsymbol{r}). \tag{15}$$

In the case of J aggregates, where $\bar{C}(\boldsymbol{r})$ is uniformly positive, the 0-0 peak is a direct measure of the coherence size and is the source of superradiance [see Eq. (13) with $|\bar{C}(\boldsymbol{r})| = \bar{C}(\boldsymbol{r})$]. Since the side-band line strengths are largely incoherent, the ratio $I_{\mathrm{PL}}^{0\text{-}0}/I_{\mathrm{PL}}^{0\text{-}1}$, is useful for probing coherence. In Ref. 44, we obtained the simple relationship

$$I_{\mathrm{PL}}^{0\text{-}0}/I_{\mathrm{PL}}^{0\text{-}1} \approx N_{\mathrm{coh}}/\lambda^2. \tag{16}$$

Equation (15) provides a simple means of extracting N_{coh} directly from the PL spectrum in J aggregates.[35,44]

In marked contrast, in H aggregates, the 0-0 intensity (as well as the ratio $I_{\mathrm{PL}}^{0\text{-}0}/I_{\mathrm{PL}}^{0\text{-}1}$) is *not* directly proportional to the coherence number because the phase oscillations in $C(\boldsymbol{r})$ lead to destructive interferences in $I_{\mathrm{PL}}^{0\text{-}0}$ [see Eq. (15)] but not in N_{coh} [see Eq. (13)]. As a result, in H aggregates, the PL ratio is *inversely* related to N_{coh}, decreasing with increasing N_{coh} as the destructive interference between chains becomes more effective.[23] In the limit of maximum coherence ($T = 0$ K and $\sigma = 0$ or $l_0 = \infty$), N_{coh} becomes equal to N and the PL ratio vanishes in H aggregates—there is no 0-0 peak by symmetry. By contrast, in the same limit, the PL ratio is maximized ($=N/\lambda^2$) in J aggregates. Hence, for H aggregates,

there is no simple relationship relating the PL ratio to N_{coh}. Expressions like Eq. (3) imply that N_{coh} is a complex function of the exciton bandwidth, disorder, and the vibronic coupling. However, once a model for disorder is assumed, N_{coh} can be determined numerically from the measured PL ratio as was done in Ref. 23. Hence, for either aggregate type (H or J), $I_{PL}^{0\text{-}0}/I_{PL}^{0\text{-}1}$ provides a means of determining N_{coh}.

In the π stacks of interest here, the PL ratio is enhanced by the coherence along the polymer chain as the transition dipoles of the repeat units are aligned in-phase. However, between chains there is a phase shift (see Fig. 9), which causes destructive interference between the chains. Hence, the H-like interchain character leads to an attenuation $I_{PL}^{0\text{-}0}/I_{PL}^{0\text{-}1}$. In the presence of disorder and thermal fluctuations, the overall PL ratio is therefore due to a *competition* between intrachain, J-favoring interactions and interchain, H-favoring interactions. As we have shown here, in P3HT films, the competition is also a function of the chain conformation dictated by the material's molecular weight, with the most influential factor being the diminished interchain coupling (and enhanced intrachain coupling) experienced by the more planar (torsionally less disordered) macromolecules of P3HT of higher M_w.

IV. DISCUSSION

From the work presented in Sec. III, we identify a clear microstructure-dependent interplay of intermolecular and intramolecular exciton spatial coherence in neat regioregular P3HT, which we rationalize in terms of a hybrid HJ-aggregate model. We can summarize the important conclusions as follows: (i) the photophysics of P3HT films results from a competition of intrachain π-electron coupling (J-aggregate-like behavior) and interchain Coulombic coupling (H-aggregate behavior); (ii) while the ratio of the 0-0 and 0-1 PL intensities is sensitive to interchain exciton coherence, the 0-2/0-1 ratio in the PL spectrum is predominantly an intrachain property that determines the effective single-chain Huang-Rhys factor λ_{eff}^2 [see Eq. (10)]. The measured change in λ_{eff}^2 from near unity in P3HT samples of high M_w to approximately 1.3–1.5 in low-M_w materials reflects greater intrachain coupling in P3HT of high M_w, which we attribute to reduced torsional disorder; (iii) the enhanced 0-0/0-1 PL ratio in films of P3HT of higher M_w is mainly due to decreased interchain couplings, which correlate to longer conjugation lengths (and coherence lengths) within the chains. Enhanced intrachain coupling also favors a larger 0-0/0-1 PL ratio; (iv) for both P3HT of high and low M_w, the coherence length is larger along the chain than across chains, but the coherence lengths do not dramatically differ between materials of low and high M_w.

We expect that the interplay between inter- and intrachain interactions is a general property in polymeric semiconductors. For instance, Köhler *et al.* recently presented convincing evidence of a second-order phase transition in MEH-PPV dissolved in methyltetrahydrofuran,[2] where the disordered "blue phase" is converted to the aggregate "red phase" as the temperature is lowered through the critical temperature near 200 K. In contrast to the PL line shape of the P3HT film aggregates studied here, the PL spectrum from red-phase MEH-PPV aggregates is dominated by the 0-0 transition, indicative of J-aggregate-like behavior resulting from dominant intrachain interactions. In fact, the spectra closely resemble the PL spectra obtained from the P3HT whiskers of Niles *et al.*,[1] the optical behavior of which was also rationalized in the same way. It is not fully understood why the optical properties of P3HT films cast from organic solvents under ambient conditions should more closely resemble H aggregates, but the work here supports the hypothesis that such aggregates are comprised of chains with more torsional disorder, shorter conjugation lengths, and therefore stronger interchain interactions. The correlation between increased intrachain spatial coherence and reduced interchain coupling is consistent with the well-known oligomer length effect: the longer the oligomer, the weaker are the interchain excitonic couplings.[39–41]

The solid-state microstructures formed over the wide molecular weight range studied in this work are very distinct, ranging from a one-phase, chain extended (paraffinic-like) structure to a two-phase semicrystalline morphology,[16] and the absorbance and PL spectral line shapes vary accordingly (see Figs. 1 and 2). It is striking that while field-effect mobilities,[12–16] time-of-flight mobilities,[16,17] and microwave conductivities[3] all display marked dependence on microstructure, the two-dimensional equilibrium exciton spatial coherence function derived from analysis of the PL spectral lines shape varies in a modest way over the same range (see Figs. 8 and 9). This reflects the strong Frenkel-like character of excitons in P3HT, which, together with the strong coupling to vibrational degrees of freedom and the substantial amount of configurational disorder intrinsic in these semicrystalline microstructures, results in fairly strong localization. From Fig. 8, we obtain a coherence "area"—defined as the product of the two coherence lengths in Eqs. (14a) and (14b)—of roughly 130 Å^2 for both low- and high-M_w materials, with P3HT of high M_w being slightly more anisotropic ("rectangular"). We have focused mainly on the steady-state exciton coherence, although our time resolved results in Fig. 3 indicate that for time windows beyond the ~200 fs time resolution of our experiment, the spatial coherence properties do not change significantly in P3HT of high M_w. In contrast, the significant reduction in the PL 0-0/0-1 ratio with time over the first 5–10 ps in materials of low M_w is consistent with an increasing coherence domain size with time due to planarization of the more torsionally disordered P3HT chains.[47] Interestingly, Banerji *et al.* reported that in films based on P3HT of $M_w = 79.9$ kg/mol, this relaxation of the 0-0 intensity on picosecond timescales takes the system from a predominantly J-like emission spectrum (the 0-0 peak is *more* intense than the 0-1 peak), to distinctly an H-like emission spectrum (suppressed 0-0 intensity with respect to the rest of the progression).[48] We speculate that at early time, well within the time resolution of most ultrafast experiments ($\ll$100 fs), nascent excitons are characterized by long coherence before localization occurs to produce the the coherence lengths at equilibrium conditions, as discussed in this work. Such a scenario involving spatially coherent excitation at organic heterojunctions in the photocarrier photogeneration mechanism in solar cells has received significant support in the last year.[48,56] Interestingly, photovoltaic efficiency performance in P3HT:PCBM diodes is found to be optimized with P3HT of medium M_w,[57] and we propose that early-time spatial coherence properties of polymer films may depend

on the complex configurational and energetic landscape in similar ways as the equilibrium spatial coherence properties investigated here. We consider that this is a valuable future direction of research using techniques such as multidimensional electronic spectroscopy.

V. CONCLUSION

In this paper, we have shown how to analyze the steady-state photoluminescence spectral line shape in order to obtain the two-dimensional exciton coherence function in semicrystalline polymeric semiconductors. In particular, the 0-0/0-1 PL ratio results from a competition between intrachain interactions, which serve to enhance the PL ratio (as is characteristic of J aggregates) and interchain interactions, which serve to attenuate the PL ratio (as is characteristic of H aggregates). The resulting coherence function for P3HT π stacks is J-like (nodeless) along the chain, and H-like (oscillating phase) across the chains. By contrast, the 0-2/0-1 PL ratio, quantifying the effective Huang-Rhys parameter of the vibronic progression, is sensitive primarily to intrachain excitonic coupling. In regioregular P3HT films, the interplay between intra- and intermolecular interactions results in a coherence "area" of approximately 130 Å^2. Low-molecular-weight ($M_w < 50$ kg/mol) materials form chain-extended morphologies based on lamellar stacks of torsionally disordered macromolecules, leading to excitons with interchain spatial coherence that extends over ∼10 Å (i.e., over 2.5 neighboring macromolecules), but with intrachain spatial coherence limited to ∼13 Å (i.e., ≈3 thiophene monomers). On the opposite regime, films made of high-molecular-weight P3HT ($M_w > 50$ kg/mol), which are characterized by two-phase morphologies consisting of interconnected crystalline and amorphous domains, host excitons that are spatially coherent over only ∼7.5 Å along the stacking axis, but over ∼18 Å along the chain. Hence the coherence areas for P3HT of low and high M_w are similar, although high-M_w materials host a more anisotropic coherence favored along the polymer chain axis. This establishes that there is a microstructure-dependent interplay between intrachain and interchain exciton interactions in this important class of semiconductor materials. Future work will be directed at exploring the time dependence of the spatial coherence as tracked by the time-resolved PL line shape.

ACKNOWLEDGMENTS

We acknowledge the participation of the late Gianluca Latini towards the intellectual development of this work. We acknowledge gratefully Felix Koch and Paul Smith for supply of materials and for discussions leading to the development of the polymer science reported in this paper. C.S. acknowledges funding from the Natural Sciences and Engineering Research Council of Canada (NSERC), the Fonds du Quebec de Recherche- Nature et Technologies (FRQNT), the Canada Research Chair in Organic Semiconductor Materials, and the Leverhulme Trust. N.S. is supported by a European Research Council (ERC) Starting Independent Researcher Fellowship under the Grant Agreement No. 279587. F.S. acknowledges support by the National Science Foundation under the Grant No. DMR-1203811. S.A.H. acknowledges financial support from the Engineering and Physical Science Research Council (EPSRC) through the UK-India (EP/H040218/2) program. We acknowledge support from the Royal Society through award of a University Research Fellowship (S.A.H.). N.B. and M.C. thank the NSERC and FRQNT for financial support, and Compute Canada for the computational ressources.

*spano@temple.edu

†Visiting Professor (Experimental Solid-State Physics), Department of Physics, Imperial College London, South Kensington Campus, London SW7 2AZ, United Kingdom; carlos.silva@umontreal.ca.

[1]E. T. Niles, J. D. Roehling, H. Yamagata, A. J. Wise, F. C. Spano, A. J. Moule, and J. K. Grey, J. Phys. Chem. Lett. **3**, 259 (2012).

[2]A. Kohler, S. T. Hoffmann, and H. Bassler, J. Am. Chem. Soc. **134**, 11594 (2012).

[3]O. G. Reid, J. A. N. Malik, G. Latini, S. Dayal, N. Kopidakis, C. Silva, N. Stingelin, and G. Rumbles, J. Polym. Sci. Pt. B-Polym. Phys. **50**, 27 (2012).

[4]C. Scharsich, R. H. Lohwasser, M. Sommer, U. Asawapirom, U. Scherf, M. Thelakkat, D. Neher, and A. Kohler, J. Pol. Sci. B **50**, 442 (2012).

[5]J. Clark, J. F. Chang, F. C. Spano, R. H. Friend, and C. Silva, Appl. Phys. Lett. **94**, 163306 (2009).

[6]J. Clark, C. Silva, R. H. Friend, and F. C. Spano, Phys. Rev. Lett. **98**, 206406 (2007).

[7]M. Baghgar, J. Labastide, F. Bokel, I. Dujovne, A. McKenna, A. M. Barnes, E. Pentzer, T. Emrick, R. Hayward, and M. D. Barnes, J. Phys. Chem. Lett. **3**, 1674 (2012).

[8]P. Kohn, S. Huettner, H. Komber, V. Senkovskyy, R. Tkachov, A. Kiriy, R. H. Friend, U. Steiner, W. T. S. Huck, J.-U. Sommer, and M. Sommer, J. Am. Chem. Soc. **134**, 4790 (2012).

[9]S. T. Turner, P. Pingel, R. Steyrleuthner, E. J. W. Crossland, S. Ludwigs, and D. Neher, Adv. Funct. Mater. **21**, 4640 (2011).

[10]M. Brinkmann, J. Poly. Sci. B: Poly. Phys. **49**, 1218 (2011).

[11]B. Wunderlich, *Macromolecular Physics*, Vol. 2 (Academic Press, New York, 1976).

[12]R. J. Kline, M. D. McGehee, E. N. Kadnikova, J. S. Liu, and J. M. J. Frechet, Adv. Mater. **15**, 1519 (2003).

[13]R. J. Kline, M. D. McGehee, E. N. Kadnikova, J. S. Liu, J. M. J. Frechet, and M. F. Toney, Macromolecules **38**, 3312 (2005).

[14]C. Goh, R. J. Kline, M. D. McGehee, E. N. Kadnikova, and J. M. J. Frechet, Appl. Phys. Lett. **86**, 122110 (2005).

[15]R. Zhang, B. Li, M. C. Iovu, M. Jeffries-El, G. Sauve, J. Cooper, S. J. Jia, S. Tristram-Nagle, D. M. Smilgies, D. N. Lambeth, R. D. McCullough, and T. Kowalewski, J. Am. Chem. Soc. **128**, 3480 (2006).

[16]F. P. V. Koch, J. Rivnay, S. Foster, C. Müller, J. Downing, E. Buchaca-Domingo, P. Westacott, L. Yu, M. Yuan, M. Baklar, Z. Fei, C. Luscombe, M. McLachlan, M. Heeney, G. Rumbles,

C. Silva, A. Salleo, J. Nelson, P. Smith, and N. Stingelin, Prog. Polym. Sci., doi: 10.1016/j.progpolymsci.2013.07.009.
[17]A. M. Ballantyne, L. Chen, J. Dane, T. Hammant, F. M. Braun, M. Heeney, W. Duffy, I. McCulloch, D. D. C. Bradley, and J. Nelson, Adv. Funct. Mater. **18**, 2373 (2008).
[18]M. Brinkmann and P. Ramnou, Adv. Funct. Mater. **17**, 101 (2007).
[19]E. Collini and G. D. Scholes, Science **323**, 369 (2009).
[20]C. Smyth, F. Fassioli, and G. D. Scholes, Philos. Trans. R. Soc., A **370**, 3728 (2012).
[21]O. Kuhn and V. Sundstrom, J. Chem. Phys. **107**, 4154 (1997).
[22]T. Meier, V. Chernyak, and S. Mukamel, J. Phys. Chem. B **101**, 7332 (1997).
[23]F. C. Spano, J. Clark, C. Silva, and R. H. Friend, J. Chem. Phys. **130**, 074904 (2009).
[24]F. C. Spano, Acc. Chem. Res. **43**, 429 (2010).
[25]R. Osterbacka, C. P. An, X. M. Jiang, and Z. V. Vardeny, Science **287**, 839 (2000).
[26]H. Sirringhaus, P. J. Brown, R. H. Friend, M. M. Nielsen, K. Bechgaard, B. M. W. Langeveld-Voss, A. J. H. Spiering, R. A. J. Janssen, E. W. Meijer, P. Herwig, and D. M. de Leeuw, Nature (London) **401**, 685 (1999).
[27]F. C. Spano, J. Chem. Phys. **122**, 234701 (2005).
[28]F. C. Spano, Chem. Phys. **325**, 22 (2006).
[29]C. Hellman, F. Paquin, N. D. Treat, A. Bruno, L. X. Reynolds, S. A. Haque, P. Stravrinou, C. Silva, and N. Stingelin [Adv. Mater. (to be published)].
[30]W. Barford, *Electronic and Optical Properties of Conjugated Polymers* (Clarendon Press, Oxford, 2005).
[31]A. Horvath, G. Weiser, C. Lapersonne-Meyer, M. Schott, and S. Spagnoli, Phys. Rev. B **53**, 13507 (1996).
[32]R. Lecuiller, J. Berrehar, J. D. Ganiere, C. Lapersonne-Meyer, P. Lavallard, and M. Schott, Phys Rev. B **66**, 125205 (2002).
[33]F. Dubin, R. Melet, T. Barisien, R. Grousson, L. Legrand, M. Schott, and V. Voliotist, Nat. Phys. **2**, 32 (2006).
[34]M. Schott, in *Photophysics of Molecular Materials: from Single Molecules to Single Crystals*, edited by G. Lanzani (Wiley-VCH, Weinheim, 2006), p. 49.
[35]H. Yamagata and F. C. Spano, J. Chem. Phys. **135**, 054906 (2011).
[36]H. Yamagata and F. C. Spano, J. Chem. Phys. **136**, 184901 (2012).
[37]S. Westenhoff, A. Abrusci, W. J. Feast, O. Henze, A. F. M. Kilbinger, A. Schenning, and C. Silva, Adv. Mater. **18**, 1281 (2006).
[38]J. Gierschner, Y. S. Huang, B. Van Averbeke, J. Cornil, R. H. Friend, and D. Beljonne, J. Chem. Phys. **130**, 044105 (2009).
[39]W. Barford, J. Chem. Phys. **126**, 134905 (2007).
[40]J. Cornil, D. A. dos Santos, X. Crispin, R. Silbey, and J. L. Bredas, J. Am. Chem. Soc. **120**, 1289 (1998).
[41]E. S. Manas and F. C. Spano, J. Chem. Phys. **109**, 8087 (1998).
[42]C. Groves, O. G. Reid, and D. S. Ginger, Acc. Chem. Res. **43**, 612 (2010).
[43]See Supplemental Material at http://link.aps.org/supplemental/10.1103/PhysRevB.88.155202 for the analysis of W for a Huang-Rhys parameter different than 1, comparison of the theoretical absorption spectrum within the H- and HJ-aggregate model, and calculation of the Huang-Rhys parameter of a single thiophene unit.
[44]K. Kanemoto, T. Sudo, I. Akai, H. Hashimoto, T. Karasawa, Y. Aso, and T. Otsubo, Phys. Rev. B **73**, 235203 (2006).
[45]F. C. Spano and H. Yamagata, J. Phys. Chem. B **115**, 5133 (2011).
[46]R. Chang, J. H. Hsu, W. S. Fann, K. K. Liang, C. H. Chiang, M. Hayashi, J. Yu, S. H. Lin, E. C. Chang, K. R. Chuang, and S. A. Chen, Chem. Phys. Lett. **317**, 142 (2000).
[47]J. Cornil, D. Beljonne, C. M. Heller, I. H. Campbell, B. K. Laurich, D. L. Smith, D. D. C. Bradley, K. Mullen, and J. L. Bredas, Chem. Phys. Lett. **278**, 139 (1997).
[48]P. Parkinson, C. Mueller, N. Stingelin, M. B. Johnston, and L. M. Herz, J. Phys. Chem. Lett. **1**, 2788 (2010).
[49]N. Banerji, S. Cowan, E. Vauthey, and A. J. Heeger, J. Phys. Chem. C **115**, 9726 (2011).
[50]E. Busby, E. C. Carroll, E. M. Chinn, L. Chang, A. J. Moule, and D. S. Larsen, J. Phys. Chem. Lett. **2**, 2764 (2011).
[51]S. Tretiak, A. Saxena, R. L. Martin, and A. R. Bishop, Phys. Rev. Lett. **89**, 097402 (2002).
[52]E. W. Knapp, Chem. Phys. **85**, 73 (1984).
[53]F. C. Spano, S. C. J. Meskers, E. Hennebicq, and D. Beljonne, J. Am. Chem. Soc. **129**, 7044 (2007).
[54]M. Dahlbom, T. Pullerits, S. Mukamel, and V. Sundstrom, J. Phys. Chem. B **105**, 5515 (2001).
[55]T. Meier, Y. Zhao, V. Chernyak, and S. Mukamel, J. Chem. Phys. **107**, 3876 (1997).
[56]L. G. Kaake, J. J. Jasieniak, R. C. Bakus, G. C. Welch, D. Moses, G. C. Bazan, and A. J. Heeger, J. Am. Chem. Soc. **134**, 19828 (2012).
[57]W. Ma, J. Y. Kim, K. Lee, and A. J. Heeger, Macromol. Rapid Commun. **28**, 1776 (2007).